Electronic Research Archive

ERA, 33(11): 7146–7171.
DOI: 10.3934/era.2025316
Received: 11 October 2025
Revised: 08 November 2025
Accepted: 14 November 2025
Published: 24 November 2025

https://www.aimspress.com/journal/ERA

Research article

Adaptive prediction of IMQ-RBF interpolation variable shape parameters using an SSA-MLP-RF hybrid model

Junbo Yang*, Ling Wang* and Dianxuan Gong

College of Sciences, North China University of Science and Technology, Tangshan 063210, China

* **Correspondence:** Email: yangjb@stu.ncst.edu.cn, wangl1216@ncst.edu.cn.

Abstract: The shape parameter is crucial for radial basis functions (RBF) interpolation accuracy. Fixed global parameters often fail with complex data, whereas variable shape parameters improve flexibility by adjusting each basis function dynamically. To address the issue that variable shape parameter selection in the inverse multiple quadratic radial basis function (IMQ-RBF) interpolation is influenced by multiple factors, we proposed a hybrid prediction model based on the sparrow search algorithm (SSA) combining a multilayer perceptron and random forest (SSA-MLP-RF), which maps local geometric features of data points to the corresponding shape parameters. First, a dataset was constructed from scattered points, including the shape parameter values and 17 local features, to accumulate influencing factors. Subsequently, outlier removal, variance inflation factor analysis, XGBoost feature average gain, and mutual information methods were applied to perform feature selection, identifying seven key features. Finally, SSA was employed to optimize the hyperparameters of the MLP and RF, and a weighted combination model was constructed to achieve adaptive selection of shape parameters. Based on the test set results, the ablation experiments verified that the proposed SSA-MLP-RF hybrid model achieved significant performance improvement. Compared with several classical metaheuristic algorithms (particle swarm optimizatio, genetic algorithm, whale optimization algorithm, and blood-sucking leech optimizer), the SSA-MLP-RF model demonstrated the best predictive accuracy for the deformation shape parameter, achieving an R^2 of 0.9203, with MAE, RMSE, MAPE, and NMSE values of 0.0391, 0.0499, 3.8201%, and 0.0797, respectively, and a Rényi entropy of 0.1200. The findings validated the effectiveness and rationality of the proposed model, providing a reliable approach for the adaptive selection of shape parameters in RBF interpolation.

Keywords: inverse multiple quadratic radial basis function; shape parameters; sparrow search algorithm; multilayer perceptron; random forest; hybrid prediction model

1. Introduction

Radial basis function (RBF) interpolation, as a meshless method, offers advantages such as broad applicability, high accuracy, and adjustable shape parameters [1,2]. The Inverse Multiple Quadratic Radial Basis Function (IMQ-RBF) is a widely used type of RBF, which is positive definite in spaces of arbitrary dimension [3]. The rational selection of its shape parameters directly affects interpolation accuracy. Compared with globally fixed shape parameters [4,5], variable shape parameters can more precisely capture local variations in data distribution [6,7].

In recent years, numerous methods have been proposed by researchers worldwide for selecting the shape parameter in RBF interpolation. These approaches mostly include analytical and empirical methods, optimization-based search strategies [8–10], adaptive local adjustment techniques [4], and data-driven or deep learning approaches [11]. Sun and Wang [12] systematically reviewed approximately 169 related studies and pointed out that most researchers determine the shape parameter from the perspectives of error minimization, sampling density, or optimization. However, researchers focusing on the relationship between nodal geometric features and the shape parameter remain largely absent.

Motivated by this gap, we construct a deformation shape parameter prediction model from a geometric-feature perspective, mapping the spatial distribution characteristics of local nodes to their corresponding optimal shape parameters, thereby achieving adaptive prediction of RBF interpolation parameters. Figure 1 presents the flowchart of the structure of this study. This approach differs fundamentally from traditional error- or optimization-driven methods, representing a novel geometry-driven strategy to determine shape parameters. It not only addresses the limitations of existing studies but also provides a new research direction for feature-learning-based adaptive selection of RBF parameters.

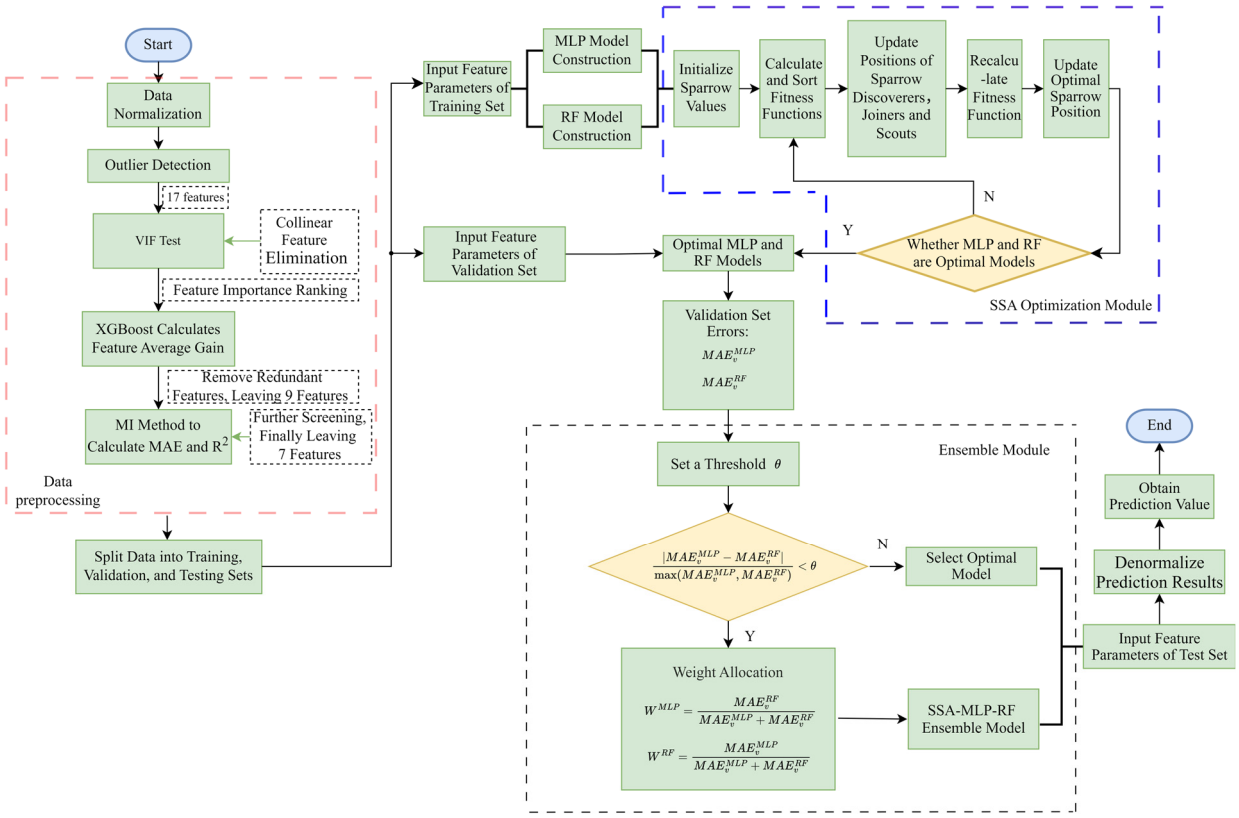

Figure 1. Flowchart of the structure of this study.

The remainder of this paper is organized as follows: In Section 2, we review the relevant literature; in Section 3, we present the underlying theory, including the principles of IMQ-RBF interpolation, the sparrow search algorithm (SSA), and data preprocessing methods; in Section 4, we describe the experiments and demonstrate the results of data preprocessing; in Section 5, we detail the construction of the adaptive selection model; in Section 6, we present the performance comparison of different models; and in Section 7, we provide the concluding remarks.

2. Related literature

Regarding the selection of fixed shape parameters in RBFs, Sun et al. [4] proposed the improved random walk algorithm and particle swarm optimization-backpropagation neural network model, to determine the optimal shape parameter in RBF interpolation and establish the quantitative relationship between angular frequency ω and c [5]. Koupaei et al. [8] applied particle swarm optimization (PSO) to optimize the shape parameters in RBF-based solutions of partial differential equations, achieving an order-of-magnitude reduction in error. Moazami and Esmaeilbeigi [9] proposed a hybrid radial kernel approach combined with PSO, which reduced the error by 1–3 orders of magnitude compared with traditional single-kernel methods when solving integral equations. González-Rodelas et al. [13] employed radial basis functions under tension (RBFT) combined with a multi-objective genetic algorithm based on NSGA-II to simultaneously optimize the number and placement of interpolation centers, achieving improved interpolation accuracy. However, this approach relies heavily on iterative search, and further research is needed to enhance interpolation efficiency and reduce computational overhead.

Researchers have proposed various methods for determining variable shape parameters [14,15]. Nojavan et al. [6] compared five variable shape parameter strategies with fixed shape parameters in solving two-dimensional nonlinear coupled Burgers equations, showing that the variable strategies yielded the smallest interpolation errors. Fornberg and Zuev [7] demonstrated that variable shape parameters improve the condition number and reduce ill-conditioning of the interpolation matrix compared to constant shape parameters. Afiatdoust and Esmaeilbeigi [10] used a genetic algorithm to determine RBF variable shape parameters and solve differential equations, achieving error reductions of 1–3 orders of magnitude compared with traditional strategies such as exponential or random approaches. Mojarrad et al. [11] employed neural networks to determine variable shape parameters in RBF interpolation, reducing errors by 1–2 orders of magnitude compared with other methods. Xiang et al. [16] introduced exponential, random, and triangular variable parameter strategies to determine the values of shape parameters. Based on these formulas, Biazar and Hosami [17] derived the optimal ranges of variable shape parameters under different data distributions. Zhu and Wathen [18] and Bozzini et al. [19] derived sufficient conditions for the uniqueness of solutions in RBF interpolation with variable shape parameters for compactly supported and global RBFs, respectively. Jankowska and Karageorghis [20] applied the Kansa RBF collocation method with variable shape parameters to solve nonlinear boundary value problems. Chiu et al. [21] proved the invertibility of Gaussian interpolation matrices with variable shape parameters and extended the results to anisotropic Gaussian kernels. Zhang et al. [22] employed a symmetric variable parameter approach combined with the ghost point method, reducing the error by 3–5 orders of magnitude. Lin et al. [23] introduced ghost points inside and outside the interpolation domain to enhance boundary interpolation accuracy without increasing computational cost. Yu et al. [24] proposed a bounded random variable parameter selection formula based on the distribution of interpolation points. Majdisova et al. [25] identified reference points such as extrema and inflection points by analyzing first-order curvature characteristics and calculated shape parameters using a formula, improving stability by at least tenfold. Gao et al. [26] established a dynamic mapping

between local point density and shape parameters and proposed a five-level parameter scaling strategy.

Bai et al. [27] proposed the blood-sucking leech optimizer (BSLO), which demonstrated excellent stability and accuracy in function optimization and parameter optimization tasks. Wei et al. [28] proposed an adaptive multi-strategy improvement to the traditional SSA. Deep learning models have attracted increasing attention in regression and interpolation studies. Convolutional neural networks (CNNs) and long short-term memory (LSTM) networks are capable of effectively capturing spatial and temporal dependencies, while transformer and graph neural network (GNN) architectures possess self-attention and relational learning capabilities [29]. These approaches exhibit outstanding performance on large-scale, high-dimensional datasets but often require complex data preprocessing, high computational costs, and long training times. In contrast, ensemble-learning-based models, when optimized through metaheuristic algorithms, can achieve comparable accuracy under small-to-moderate sample conditions and enhance the interpretability of hybrid frameworks through multi-metric performance evaluations. Therefore, we focus on an ensemble framework enhanced by a metaheuristic algorithm, which constructs a deformation shape parameter selection model based on geometric features.

3. Theoretical analysis

The theoretical analysis in this section focuses on the core supporting theories of the proposed SSA multilayer perceptron and random forest (SSA-MLP-RF) model, covering the fundamental principle of IMQ-RBF interpolation (the basis for shape parameter optimization), the optimization mechanism of the SSA, and the implementation logic of data preprocessing and ensemble learning. These contents collectively provide a rigorous theoretical foundation for the subsequent model construction and experimental validation.

3.1. Theory of IMQ-RBF interpolation

A RBF is a real-valued function ϕ whose value depends solely on the distance from the origin, i.e., $\Phi(x)=\phi\left(\|x\|,c\right)$. If the condition $\|x_1\|=\|x_2\|$ is satisfied, then $\phi\left(\|x_1\|,c\right)=\phi\left(\|x_2\|,c\right)$. The IMQ-RBF interpolation is defined as follows [1]:

$$f(x_i)=\sum_{j=1}^{N}\alpha_j\phi(r_{ij},c_j)=\sum_{j=1}^{N}\alpha_j\phi\left(\left\|x_i-x_j\right\|_2,c_j\right),\quad i=1,2,...,N. \tag{1}$$

In the above equation,

$$\phi(r_{ij},c_j)=\frac{1}{\sqrt{(x_i-x_j)^2+c_j^2}}, \tag{2}$$

represents the RBF centered at point x_j with c_j as the shape parameter. Here, $\left\|x_i-x_j\right\|_2$ denotes the Euclidean distance between the interpolation point x_i and the reference point x_j; N is the total number of sampling points; and α_j is the interpolation coefficient, representing the weight of the j-th reference point.

Its matrix form can be expressed as:

$$f=\Psi_{Var}\alpha, \tag{3}$$

where

$$\alpha = \left[\alpha_1, \alpha_2, \cdots, \alpha_N\right]^T,$$

$$f = \left[f(x_1), f(x_2), \cdots, f(x_N)\right]^T,$$

$$\Psi_{Var} = \begin{pmatrix} \phi(r_{11}, c_1) & \cdots & \phi(r_{1N}, c_N) \\ \vdots & \ddots & \vdots \\ \phi(r_{N1}, c_1) & \cdots & \phi(r_{NN}, c_N) \end{pmatrix}.$$

3.2. Sparrow search algorithm

In the SSA, sparrows are categorized as discoverers, joiners, and scouts. In the problem of determining the optimal variable shape parameters for RBFs, each sparrow represents a candidate set of shape parameters [28]. When optimizing the hyperparameters of MLP and RF models, each sparrow corresponds to a set of hyperparameters to be optimized. During the iterative update process, the fitness of each individual is evaluated by computing the root mean square error (RMSE) between predicted and actual values.

1) Position update equation for discoverers:

$$X_{i,j}^{t+1} = \begin{cases} X_{i,j}^{t} \cdot \exp\left(-\dfrac{i}{\alpha \cdot iter_{\max}}\right) & if\ R_2 < ST \\ X_{i,j}^{t} + Q \cdot L & if\ R_2 \geq ST \end{cases}. \tag{4}$$

In Eq (4), $X_{i,j}^{t}$ is the position of the current discoverer at the t-th iteration. α is a random number in the range [0,1], $iter$ is the current iteration number, and $iter_{\max}$ is the maximum number of iterations. R_2 is a random number in the range [0,1] representing the early - warning value. ST is a constant in the range [0.5,1], representing the safety threshold of the discoverer. Q is a random number following a normal distribution. L is a $1 \times d$ matrix with all elements being 1. When $R_2 < ST$, the discoverer performs a global search with a relatively large step size to explore new regions. Conversely, when $R_2 \geq ST$, the discoverer focuses on local exploitation by fine-tuning its position to further optimize the solution.

2) Position update equation for joiners:

$$X_{i,j}^{t+1} = \begin{cases} Q \cdot \exp\left(\dfrac{X_{worst}^{t} - X_{i,j}^{t}}{i^2}\right) & if\ i > n/2 \\ X_{P}^{t+1} + \left|X_{i,j}^{t} - X_{P}^{t+1}\right| \cdot A^{+} \cdot L & otherwise \end{cases}. \tag{5}$$

In Eq (5), X_{worst}^{t} denotes the position of the worst-performing individual in the population at iteration t, and X_{P}^{t+1} is the optimal position among the discoverers. $A^{+} = A^{T}\left(AA^{T}\right)^{-1}$ is the coefficient related to the joiners, where A is a $1 \times d$ matrix with elements being 1 or –1. When $i > n/2$ (where n is the total population size), the joiners with lower fitness values perform a long-distance search toward better-performing individuals, facilitating global exploration. Otherwise, the

joiners conduct a local search around the current best position to further refine the solution and improve convergence accuracy.

3) Position update equation for scouts:

$$X_{i,j}^{t+1} = \begin{cases} X_{best}^{t} + \beta \cdot \left| X_{i,j}^{t} - X_{best}^{t} \right| & if\ f_i > f_g \\ X_{i,j}^{t} + K \cdot \left(\dfrac{\left| X_{i,j}^{t} - X_{worst}^{t} \right|}{(f_i - f_w) + \varepsilon} \right) & if\ f_i = f_g \end{cases}. \tag{6}$$

In Eq (6), X_{best}^{t} denotes the current global best position in the population. β is a scout-related coefficient. f_i is the fitness of the current individual, and f_g and f_w represent the fitness values of the best and worst individuals in the population, respectively. K is a random number uniformly distributed in the interval [–1,1], where its sign indicates the direction of the scout's movement and its magnitude controls the step size. ε is a very small constant used to avoid division by zero. If the fitness of the current individual differs from the optimal fitness, scouts move toward the optimal positions, guiding the population in a better search direction; otherwise, they move randomly to avoid being trapped in local optima.

3.3. Outlier removal

To ensure data comparability and eliminate scale bias, all 17 features are first subjected to logarithmic transformation and standardization. Subsequently, violin plots are used to visualize the distribution and density of each feature, enabling the identification and removal of samples that significantly deviate from the normal range, thereby improving data reliability and stability.

3.4. Variance inflation factor

In the problem of predicting variable shape parameters for RBF interpolation, feature redundancy may lead to model instability and reduced prediction accuracy. The variance inflation factor (VIF) is introduced to quantitatively assess multicollinearity. VIF measures the degree of linear correlation between a given feature and the remaining features. The calculation procedure is as follows:

The i-th feature X_i is treated as the dependent variable, while the remaining 16 features $\{X_1,...,X_{i-1},X_{i+1},...,X_{17}\}$ are treated as independent variables to construct a linear regression model:

$$X_i = \beta_0 + \sum_{j \neq i} \beta_j X_j + \epsilon\,. \tag{7}$$

The coefficient of determination reflects the strength of the linear relationship between the feature and the others, and is defined as:

$$R_i^2 = 1 - \frac{\sum_{k=1}^{n} \left(X_{ik} - \hat{X}_{ik} \right)^2}{\sum_{k=1}^{n} \left(X_{ik} - \bar{X}_i \right)^2}. \tag{8}$$

Here, X_{ik} denotes the k-th sample value of the i-th feature; $\hat{X}_{ik}$ is the regression-predicted

value; $\bar{X}_i$ is the mean of the feature; and n is the total number of samples.

Based on R_i^2, the VIF of the i-th feature is calculated as:

$$VIF_i = \frac{1}{1-R_i^2}. \tag{9}$$

A feature is generally considered to exhibit severe multicollinearity if $VIF_i > 10$ and should be removed. By calculating VIF values for all features and eliminating redundant variables, the correlation among features can be effectively reduced, thereby improving the stability and generalization capability of the RBF variable shape parameter prediction model.

3.5. Feature average gain calculation using XGBoost

XGBoost is a gradient boosting tree (GBT) ensemble model that has demonstrated excellent generalization performance in various prediction tasks. The model iteratively fits the residuals of the previous round, thereby progressively reducing the model error. For feature importance evaluation, XGBoost provides multiple metrics. The split count (FScore) indicates the frequency with which a feature is used for splitting across all trees, while the average gain (AverageGain) measures the average decrease in the objective function brought by the feature during splits. Since we focus on the actual contribution of features to the prediction performance of RBF variable shape parameters, AverageGain is employed as the primary importance metric, with FScore serving as a supplementary verification.

Let the sample set be $D = \{(x_i, c_i)\}_{i=1}^m$, where each sample $x_i \in \mathbb{R}^{17}$ is the local feature vector of the i-th scattered point, and the target variable $c_i \in \mathbb{R}$ represents the IMQ-RBF variable shape parameter of that point. Denote the t-th tree trained by XGBoost as $f_t(\cdot)$; the model prediction after T rounds is given by:

$$\hat{c}_i^{(T)} = \sum_{t=1}^{T} f_t(x_i). \tag{10}$$

The objective function optimized by XGBoost in the t-th round is:

$$Obj^{(t)} = \sum_{i=1}^{m} l\left(c_i, \hat{c}_i^{(t-1)} + f_t(x_i)\right) + \Omega(f_t). \tag{11}$$

Here, $l(\cdot,\cdot)$ denotes the per-sample loss; $\Omega(f) = \gamma T_f + \frac{1}{2}\lambda \sum_j w_j^2$ represents the regularization on tree complexity; T_f is the number of tree leaves; ω_j is the weight of the j-th leaf; and $\gamma, \lambda \geq 0$ denotes the hyperparameters.

For each sample, a second-order Taylor expansion of $f_t(x_i)$ at the current prediction point yields:

$$l\left(c_i, \hat{c}_i^{(t-1)} + f_t(x_i)\right) \approx l\left(c_i, \hat{c}_i^{(t-1)}\right) + g_i f_t(x_i) + \frac{1}{2} h_i f_t^2(x_i), \tag{12}$$

where

$$g_i \equiv \frac{\partial l\left(c_i, \hat{y}\right)}{\partial \hat{y}}\Big|_{\hat{y}=\hat{c}_i^{(t-1)}}, \tag{13}$$

$$h_i \equiv \frac{\partial^2 l(c_i, \hat{y})}{\partial \hat{y}^2}|_{\hat{y}=\hat{c}_i^{(t-1)}} . \tag{14}$$

Let the set of leaves of the current fitted tree f_t be L, and denote the set of samples corresponding to leaf $j \in L$ as $I_j = \{i \mid x_i \ falling\ in\ leaf\ j\}$. By substituting the Taylor expansion and retaining only the terms related to f_t, the approximate objective for a single tree is obtained as:

$$\widetilde{Obj}^{(t)} = \sum_{j \in L}\left[\sum_{i \in I_j}\left(g_i w_j + \frac{1}{2} h_i w_j^2\right)\right] + \frac{1}{2}\lambda \sum_{j \in L} w_j^2 + \gamma |L|, \tag{15}$$

where $f_t(x_i) = w_j$ on leaf j (the constant prediction value of the leaf).

The terms related to each leaf j can be organized as:

$$\widetilde{Obj}_j = w_j \sum_{i \in I_j} g_i + \frac{1}{2} w_j^2 \left(\sum_{i \in I_j} h_i + \lambda\right) + \gamma . \tag{16}$$

Taking the derivative with respect to ω_j and setting it to zero yields the optimal weight for leaf j:

$$w_j^* = -\frac{\sum_{i \in I_j} g_i}{\sum_{i \in I_j} h_i + \lambda} . \tag{17}$$

The corresponding decrease in the objective function is:

$$\widetilde{Obj}_j(w_j^*) = -\frac{1}{2}\frac{\left(\sum_{i \in I_j} g_i\right)^2}{\sum_{i \in I_j} h_i + \lambda} + \gamma . \tag{18}$$

During node splitting, if a feature k partitions node I into left and right child nodes I_L and I_R, the gain can be expressed as:

$$Gain(k) = \frac{1}{2}\left(\frac{\left(\sum_{i \in I_L} g_i\right)^2}{\sum_{i \in I_L} h_i + \lambda} + \frac{\left(\sum_{i \in I_R} g_i\right)^2}{\sum_{i \in I_R} h_i + \lambda} - \frac{\left(\sum_{i \in I} g_i\right)^2}{\sum_{i \in I} h_i + \lambda}\right) - \gamma \tag{19}$$

A split is accepted and can improve model fitting if $Gain > 0$.

During training, if feature $k \in \{1, \ldots, 17\}$ is used $|S_k|$ times across all trees and splits, and the gain for each split is denoted as $Gain_{k,r}$ over $r \in S_k$ splits, its average gain is defined as:

$$AverageGain_k = \frac{1}{|S_k|}\sum_{r \in S_k} Gain_{k,r} . \tag{20}$$

If $|S_k|=0$, let $AverageGain_k=0$. Finally, features are ranked comprehensively using AverageGain and FScore to identify the key factors that contribute most significantly to RBF variable shape parameter prediction.

3.6. Feature selection using mutual information

In probability and information theory, mutual information (MI) quantifies the dependency between two random variables. Unlike correlation coefficients, MI is applicable not only to real-valued random variables but also captures linear and nonlinear relationships between variables. Let the joint probability distribution of random variables X and Y be $p_{XY}(x,y)$, and the marginal distributions be $p_X(x)$ and $p_Y(y)$; then MI is defined as:

$$I(X;Y)=\sum_{y\in Y}\sum_{x\in X}p(x,y)\log_2\left(\frac{p(x,y)}{p(x)p(y)}\right). \tag{21}$$

For continuous random variables, the summation is replaced by an integral:

$$I(X;Y)=\int_Y\int_X p(x,y)\log_2\left(\frac{p(x,y)}{p(x)p(y)}\right)\mathrm{d}x\mathrm{d}y. \tag{22}$$

MI possesses non-negativity, symmetry, and extremal properties, and can be related to entropy:

$$\begin{aligned} I(X;Y)&=H(X)-H(X\mid Y)\\ &=H(Y)-H(Y\mid X)\\ &=H(X)+H(Y)-H(X,Y)\\ &=H(X,Y)-H(X\mid Y)-H(Y\mid X). \end{aligned} \tag{23}$$

Here, $H(X)$ and $H(Y)$ denote the marginal entropies of random variables X and Y, respectively, and $H(Y\mid X)$ is the conditional entropy, representing the uncertainty of Y given X:

$$H(Y\mid X)=-\sum_{x,y}p(x,y)\log_2\left(p(x\mid y)\right). \tag{24}$$

The MI-based feature selection method can be used to eliminate redundant features and reduce sample dimensionality. Let the set of influencing feature variables be $C_i=\left(C_{i1},C_{i2},C_{i3},\cdots,C_{i9}\right)$ and $i=1,...,n$, and the target variable be ε_i. The procedure is as follows:

Step 1: Compute the MI between each feature and the target variable.

Step 2: Rank the features in descending order of MI and select the top k features as the key influencing factors for subsequent modeling.

This method simultaneously considers linear and nonlinear dependencies, ensuring that the selected features provide high information content for predicting the target while reducing redundancy.

3.7. MLP-RF ensemble model

The MLP-RF ensemble model integrates the nonlinear fitting capability of MLP and the robustness of RF to enhance shape parameter prediction performance. To clarify the construction logic

of the integrated model, the working principles of the two base models and the development of the SSA-MLP-RF prediction model are described below.

3.7.1. MLP model principle

The MLP is a typical feedforward neural network, and its basic structure is illustrated in Figure 2. The MLP consists of multiple layers of neurons, with each layer containing several neurons equipped with nonlinear activation functions to enhance the network's nonlinear fitting capability.

Assume the network has L layers. The connection parameters between the l-th layer and the $l+1$-th layer are represented by the weight matrix w_l and bias vector b_l. Let P_l denote the input and O_l the output of the l-th layer, with the mapping relationship implemented by a function f.

In this study, the input feature vector x represents the seven factors influencing the IMQ-RBF variable shape parameter, while the output $\hat{y}$ corresponds to the model-predicted variable shape parameter. The true variable shape parameter is denoted as y.

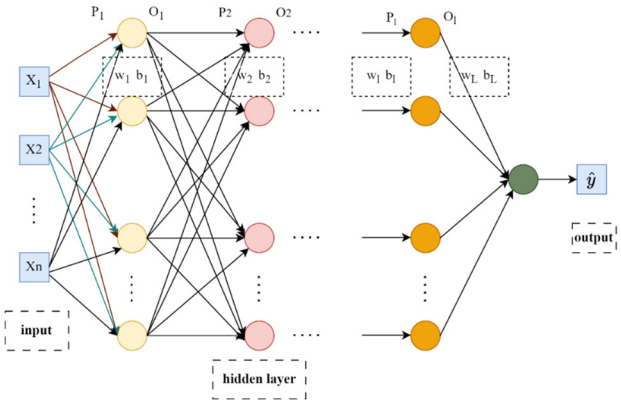

Figure 2. Framework of the MLP model.

The forward propagation process is formulated as:

$$P_l = O_{l-1} \times W_l + b_l, \tag{25}$$

$$O_l = f(P_l). \tag{26}$$

The objective function is expressed as:

$$S = (y - \hat{y})^2. \tag{27}$$

In the backpropagation stage, the gradient descent method is applied. Let $d(w_l)$ denote the gradient of the objective function with respect to w_l, $d(b_l)$ denote the gradient with respect to b_l, and h represent the learning rate. $d(O_l)$ corresponds to the derivative of the objective function with respect to the activation function in the l-th layer.

$$d(b_l) = d(b_{l+1}) \times w_{l+1} \cdot d(O_l), \tag{28}$$

$$d(w_l) = d(b_l) \times O_{l-1}. \tag{29}$$

The parameters are updated using the gradient descent rule as follows:

$$b_l' = b_l - h \cdot d(b_l), \tag{30}$$

$$w_l' = w_l - h \cdot d(w_l). \tag{31}$$

3.7.2. Principle of the random forest method

The RF algorithm is a nonparametric learning method based on the ensemble tree concept. Its core idea is to construct and integrate multiple decision trees to perform prediction tasks. The overall framework of the RF model is illustrated in Figure 3.

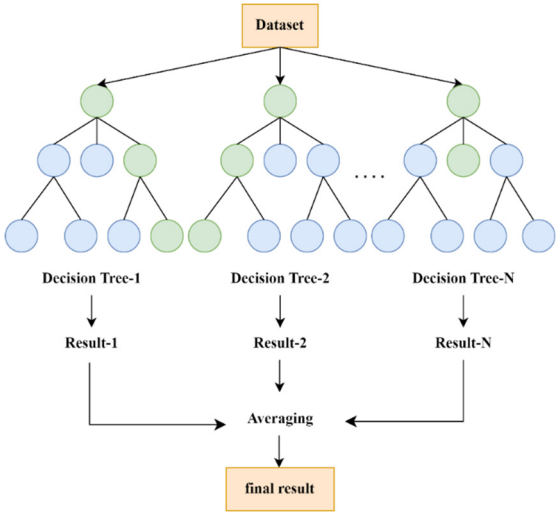

Figure 3. Framework of the RF model.

Let the training dataset be denoted as

$$D = \{(x_i, y_i) \mid i = 1, 2, \ldots, N\}, \tag{32}$$

where $x_i = (x_{i1}, x_{i2}, \ldots, x_{id}) \in \mathbb{R}^d$ represents the i-th sample with a d-dimensional input feature vector (in this study, $d = 7$, corresponding to the seven influencing factors of the IMQ-RBF shape parameter), and $y_i \in \mathbb{R}$ denotes the corresponding IMQ-RBF shape parameter value.

During the training phase, the RF generates M regression trees through the following steps:

The original training dataset D is resampled *with replacement* to generate M training subsets $\{D^{(1)}, D^{(2)}, \ldots, D^{(M)}\}$, each containing N samples. When constructing each tree, k candidate features ($k < d$) are randomly selected from the feature set, and the optimal split is determined based on minimizing the mean squared error. The decision tree is recursively generated using the selected samples and features until the stopping criterion is satisfied.

For the m-th regression tree, its prediction function is expressed as:

$$h_m(x) : \mathbb{R}^d \to \mathbb{R}, \quad m = 1, 2, \ldots, M. \tag{33}$$

Thus, the overall prediction function of the RF is given by:

$$\hat{y}(x) = \frac{1}{M}\sum_{m=1}^{M} h_m(x), \tag{34}$$

where $\hat{y}(x)$ denotes the predicted IMQ-RBF shape parameter corresponding to the input sample x.

3.7.3. SSA-MLP-RF prediction model

The combined prediction model is based on the MLP and RF models, integrated through a weighted combination approach. The target variable of the prediction model is the deformation shape parameter, and the feature variables are the seven selected influencing factors. The computational flow of the SSA-MLP-RF prediction model is shown in Figure 1, and the specific steps are as follows:

1) Data preprocessing.

The original sample dataset is preprocessed, mostly including data normalization, outlier detection, and feature selection.

2) Construction and optimization of individual machine learning models.

First, the dataset is divided into training, validation, and testing sets according to a 6:1:3 ratio. The MLP and RF are selected as base models. Both models are trained on the training set, and the SSA is adopted for hyperparameter optimization.

For the MLP model, the optimized hyperparameters include the number of hidden layers L_h (range 1–3, initial value 2), the number of neurons per layer n_h (range 32–256, initial value 64), and the learning rate η (range $10^{-1} \sim 10^{-4}$, initial value 0.01). For the RF model, the optimized hyperparameters include the number of trees n_{trees} (range 50–500, initial value 100), the maximum depth $\max\_depth$ (range 5–50, initial value 10), and the maximum number of features per node $\max\_features$ (range 1–7, initial value 2). The SSA algorithm initializes the population, sets the upper and lower bounds of hyperparameters and the number of iterations, and searches for the optimal hyperparameter combination to obtain the optimal MLP model f_{MLP} and RF model f_{RF}. After prediction on the validation set, the two models produce prediction results $\hat{y}_v^{MLP}$ and $\hat{y}_v^{RF}$, with corresponding validation errors MAE_v^{MLP} and MAE_v^{RF}, as calculated by the following formulas:

$$MAE_v^{MLP} = \frac{1}{N}\sum_{i=1}^{N}\left|y_i - \hat{y}_i^{MLP}\right|, \tag{35}$$

$$MAE_v^{RF} = \frac{1}{N}\sum_{i=1}^{N}\left|y_i - \hat{y}_i^{RF}\right|. \tag{36}$$

3) Construction of the combined prediction model.

First, a threshold $\theta = 0.1$ is defined, and the relative difference ratio Q between the two models is computed and compared with threshold θ. The relative difference ratio of the two models on the validation set is defined as Q:

$$Q = \frac{\left|MAE_v^{MLP} - MAE_v^{RF}\right|}{\max(MAE_v^{MLP}, MAE_v^{RF})}. \tag{37}$$

If $Q < \theta$:

$$W^{MLP} = \frac{MAE_v^{RF}}{MAE_v^{MLP} + MAE_v^{RF}}, \tag{38}$$

$$W^{RF} = \frac{MAE_v^{MLP}}{MAE_v^{MLP} + MAE_v^{RF}}. \tag{39}$$

If $Q \geq \theta$:

$$W^{MLP} = \begin{cases} 1 & MAE_v^{MLP} < MAE_v^{RF} \\ 0 & MAE_v^{MLP} > MAE_v^{RF} \end{cases}, \tag{40}$$

$$W^{RF} = 1 - W^{MLP}. \tag{41}$$

Therefore, the final model prediction result can be expressed as:

$$\hat{y} = W^{RF}\hat{y}^{RF} + W^{MLP}\hat{y}^{MLP}. \tag{42}$$

3.8. Model performance evaluation

To objectively evaluate and compare the predictive performance of the models, we comprehensively employ six evaluation metrics-R^2 (coefficient of determination), MAE (mean absolute error), RMSE (root mean square error), MAPE (mean absolute percentage error), NMSE (normalized mean square error), and Rényi entropy-to assess model performance. The calculation formulas are as follows:

$$R^2 = 1 - \frac{\sum_{i=1}^{N}(y_i - \hat{y}_i)^2}{\sum_{i=1}^{N}(y_i - \overline{y})^2}, \tag{43}$$

$$MAE = \frac{1}{N}\sum_{i=1}^{N}|y_i - \hat{y}_i|, \tag{44}$$

$$RMSE = \sqrt{\frac{1}{N}\sum_{i=1}^{N}(y_i - \hat{y}_i)^2}, \tag{45}$$

$$MAPE = \frac{1}{N}\sum_{i=1}^{N}\left|\frac{y_i - \hat{y}_i}{y_i}\right| \times 100\%, \tag{46}$$

$$NMSE = 1 - R^2, \tag{47}$$

$$H_\alpha(P) = \frac{1}{1-\alpha}\log\left(\sum_{i=1}^{m} p_i^\alpha\right), \quad \alpha > 0, \alpha \neq 1, \tag{48}$$

where N denotes the number of training samples; y_i represents the true deformation shape parameter value of the i-th input sample; $\hat{y}_i$ denotes the predicted deformation shape parameter value of the i-th input sample; and $\overline{y}$ is the mean of the true deformation shape parameter values across all input samples. $\alpha = 2$ represents the entropy order, $m = 45$ denotes the number of discrete

intervals of the residuals, $P = \{p_1, ..., p_m\}$, and p_i indicates the probability distribution of the prediction residuals. The closer the value of R^2 is to 1, and the smaller the values of MAE, RMSE, MAPE, NMSE, and Rényi entropy, the higher the prediction accuracy and the greater the model stability.

Based on the IMQ-RBF interpolation principle, SSA optimization mechanism, feature selection methods, the MLP-RF ensemble framework, and the performance evaluation criteria described in Sections 3.1–3.8, this study further clarifies the implementation workflow for the adaptive prediction of the IMQ-RBF variable shape parameter, thereby bridging the gap between theory and practical application.

In this study, the SSA was employed to determine the optimal variable shape parameters in IMQ-RBF interpolation. Each sparrow represents a candidate set of shape parameters, and the optimal set is identified through iterative convergence. This process further enables the accumulation of a dataset to explore key features influencing the shape parameter values of scattered points. Seventeen candidate features were initially collected. During feature selection, outlier removal and multicollinearity analysis using the VIF were first performed to ensure data quality and model stability. Subsequently, XGBoost feature importance and MI analysis were combined to identify seven key features affecting the IMQ-RBF shape parameters. Based on these seven critical factors, SSA was further applied to optimize the hyperparameters of the hybrid MLP-RF model, leading to the training of a more robust SSA-MLP-RF model for adaptive selection of shape parameters. To validate the optimization effectiveness, ablation experiments were conducted, and the results of six performance metrics on the test set indicate that each incremental improvement leads to enhanced model performance. Finally, by comparing the SSA-optimized hybrid model with other classical metaheuristic optimization strategies, the SSA optimization approach achieves superior prediction accuracy and stability.

The innovation of this study lies in establishing a mapping model between the local features of scattered data points and the optimal deformation shape parameter values, and constructing a two-layer optimization mechanism based on feature selection and the SSA. At the first layer, seven key local geometric features influencing the deformation shape parameter are identified through feature selection. These features accurately capture the local factors affecting the IMQ-RBF shape parameter, thereby improving data efficiency and model stability under medium-scale sample conditions. At the second layer, the SSA is employed to adaptively optimize the hyperparameters of the MLP-RF hybrid model. With its dynamic role allocation and spiral foraging strategy, SSA achieves a better balance between global exploration and local exploitation compared with traditional algorithms such as PSO, GA, WOA, and BSLO, leading to faster convergence and superior global solutions. This dual-layer framework of "feature selection + adaptive metaheuristic optimization" not only enhances the fitting accuracy and stability but also improves the interpretability of the parameter mapping process within the model.

The following sections present the experimental processing results and the model construction procedure in detail.

4. Data preprocessing results

Since Fourier series can represent almost all piecewise-smooth functions, the data in this study are generated by combining functions of type $y = a\sin(bx + c) + d$, thereby enhancing the diversity and representativeness of the dataset. The parameters a, b, c, and d are varied within reasonable ranges to cover different amplitudes and periods, further improving the model's generalization capability. A total of 100,000 sets of deformation shape parameter values and their corresponding 17 influencing factors are collected. The 17 local features listed in Table 1 systematically characterize the

properties of scattered points from geometric, statistical, and frequency perspectives, providing a comprehensive theoretical description of the local spatial and statistical characteristics of the scattered data. These 17 influencing factors are subsequently processed and screened to select the key factors for constructing the deformation shape parameter prediction model.

The raw data exhibit large feature ranges and local extrema, which are inherent characteristics of the sine function. After logarithmic transformation and standardization, the features have a mean of 0 and a variance of 1. This preprocessing retains local variation information while ensuring model training stability and usability, providing a reliable data foundation for the SSA-MLP-RF model's adaptive prediction. The detailed results are presented in Table 1.

Table 1. List of influencing factors for variable shape parameters.

No.	Influencing Factor	Original Value Range	Mean ± Standard Deviation	Standardized Value Range
C1	Minimum Nearest Neighbor Distance	0.0000–0.3067	0.0149 ± 0.0246	–1.0119–5.2230
C2	Mean Nearest Neighbor Distance	0.0042–0.6770	0.0526 ± 0.0588	–1.6829–5.6781
C3	Variance of Nearest Neighbor Distance	0.0000–0.1390	0.0016 ± 0.0049	–1.1435–4.3612
C4	Neighborhood Density	4.8299–519.1077	92.0276 ± 58.4739	–3.0648–1.9867
C5	Local Curvature	0.0000–392.9534	3.3916 ± 16.5398	–0.8794–3.0081
C6	Local Curvature Radius	0.0025–2,094,899	334.1251 ± 11889.3351	–1.4325–2.5344
C7	Variance of Neighborhood Function Values	0.0000–1.8531	0.1293 ± 0.1946	–0.9459–5.3114
C8	Absolute Value of Neighborhood Linear Fit Gradient	0.0001–48.7056	8.8477 ± 8.8972	–3.1415–2.0473
C9	Mean of Neighborhood Gradient Differences	0.0005–97.5458	9.1152 ± 15.1266	–1.2736–1.8412
C10	Mean Quadratic Polynomial Fitting Error	0.0000–0.0142	0.0010 ± 0.0013	–1.1381–3.4515
C11	Local-period-fft	0.0030–1.3270	0.0597 ± 0.0850	–1.3793–3.5237
C12	Local-period-peak	–0.4452–0.5272	0.0004 ± 0.0446	–2.6714–2.6897
C13	Mean Area of Triangles Containing the Point(tri-area-mean)	0.0000–1.3583	0.0375 ± 0.0677	–1.2107–4.5292
C14	Tri-area-min	0.0000–0.8164	0.0082 ± 0.0231	–0.9117–3.3014
C15	Tri-area-max	0.0000–2.1277	0.0810 ± 0.1455	–1.1351–3.0767
C16	Number of Triangles Connected to the Point	2.0000–40.0000	5.0727 ± 3.6709	–1.8955–1.6856
C17	Variance of Angles between Neighborhood Vectors and the Center Point Connection	0.0006–7.8475	1.9652 ± 0.5365	–4.1131–2.8931

4.1. Outlier removal results

Figure 4 illustrates the distribution of the 17 local features. The violin plots provide a visual representation of data dispersion and potential outliers. The results show that Feature 4 is concentrated around the median but exhibits a wide range of extreme values, indicating high dispersion. Features 2 and 5 have extended upper tails, while Feature 17 shows a noticeably elongated lower tail, suggesting the presence of sparse extreme outliers in these feature directions.

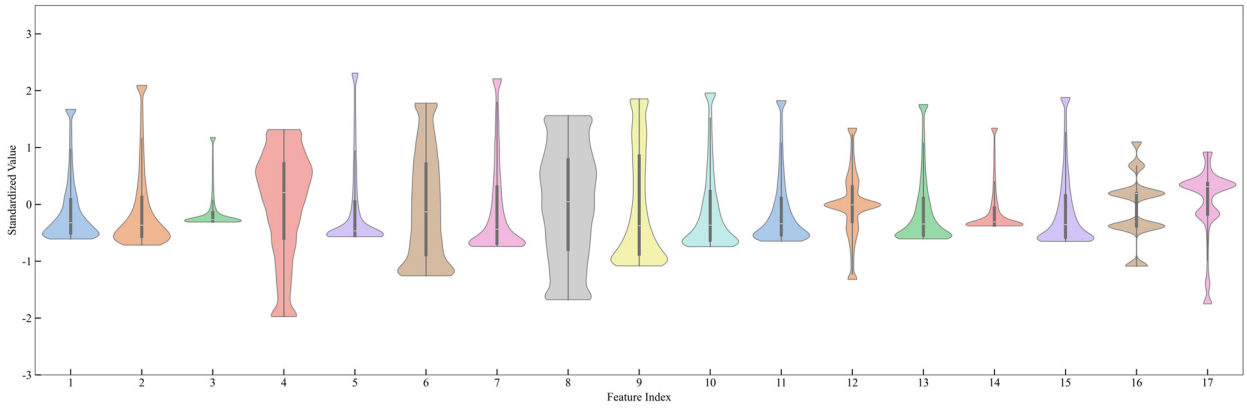

Figure 4. Violin plot of original samples.

4.2. Variance inflation factor results

Figure 5 presents the VIF values calculated for each feature. The results indicate that Features C2, C3, C4, C7, C8, C13, and C15 exhibit relatively high VIF values, suggesting a certain degree of multicollinearity. It should be noted that a high VIF does not necessarily imply that the feature must be removed; whether to retain it should be determined in combination with subsequent XGBoost feature importance rankings and MI results. This approach ensures that the selected features reduce redundancy while retaining the most informative factors for the target variable.

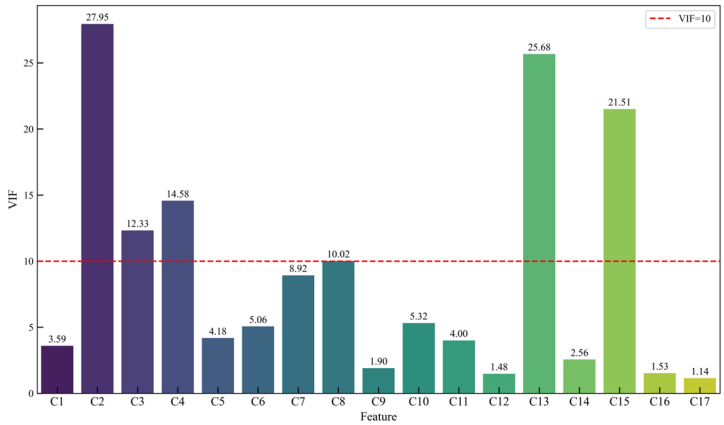

Figure 5. VIF results of influencing factors.

4.3. XGBoost feature average gain results

Table 2 presents the Average Gain and FScore values for each feature. The results indicate that Feature C4 contributes the most to predicting the variable shape parameter, with an Average Gain of 3.899 and an FScore of 442, demonstrating its significant importance in the model's splitting process. Features C2 and C5 follow, with Average Gains of 2.081 and 2.069, and corresponding FScores of 408 and 533. Among the remaining features, C8, C11, and C15 show moderate contributions, while C16, C17, and C1 exhibit low Average Gain and FScore values, indicating their relatively limited impact on prediction. Overall, the Average Gain and FScore results are consistent, highlighting C4, C2, C5, C8, C11, and C15 as the key features influencing RBF variable shape parameters, providing a reliable basis for subsequent model optimization.

Table 2. Feature importance of XGBoost ranked by average gain.

Rank	Influencing Factor	Average Gain	FScore
1	C4	3.899228	442
2	C2	2.080560	408
3	C5	2.068547	533
4	C8	2.026182	395
5	C11	1.988056	360
6	C15	1.912524	291
7	C10	1.855671	162
8	C14	1.721380	414
9	C7	1.675491	329
10	C9	1.646405	387
11	C3	1.632006	382
12	C13	1.628887	319
13	C6	1.584699	334
14	C12	1.553845	289
15	C16	1.530606	131
16	C17	1.490918	348
17	C1	1.347915	407

4.4. Feature selection results based on mutual information

Combining VIF analysis and XGBoost feature importance ranking, a systematic screening of the 17 local features is conducted. The VIF results indicate that features C2, C3, C4, C7, C8, C13, and C15 exhibited a certain degree of multicollinearity. XGBoost analysis revealed that features C2, C4, C5, and C8 contribute most significantly to predicting the RBF variable shape parameter, whereas C1, C16, and C17 have relatively low contributions. Based on these findings, nine key features, C2, C4, C5, C8, C9, C10, C11, C14, and C15, are retained for studying their nonlinear relationships with the variable shape parameter.

Using the MI function from the PyCharm neural network toolbox, the MI values between each input feature and the target variable are calculated and ranked from highest to lowest (see Figure 6). The results

show that the features ranked by descending MI are C4, C8, C10, C2, C15, C5, C11, C9, and C14, indicating a positive correlation between MI values and the features' relevance to the target variable.

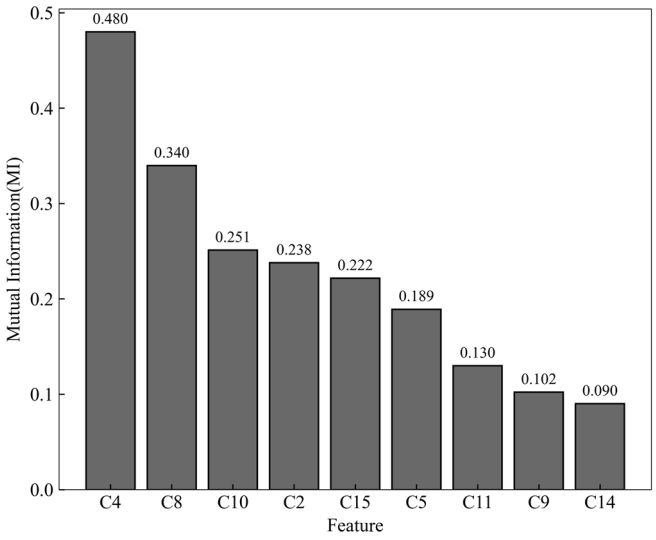

Figure 6. MI values of influencing factors.

To evaluate the impact of feature redundancy on prediction performance, the top features are selected in descending order of MI values, and an MLP-RF hybrid model is constructed for training and testing. The results indicate that prediction accuracy varies with the number of selected features (Figure 7), demonstrating that appropriate feature selection can effectively reduce redundancy and improve model performance.

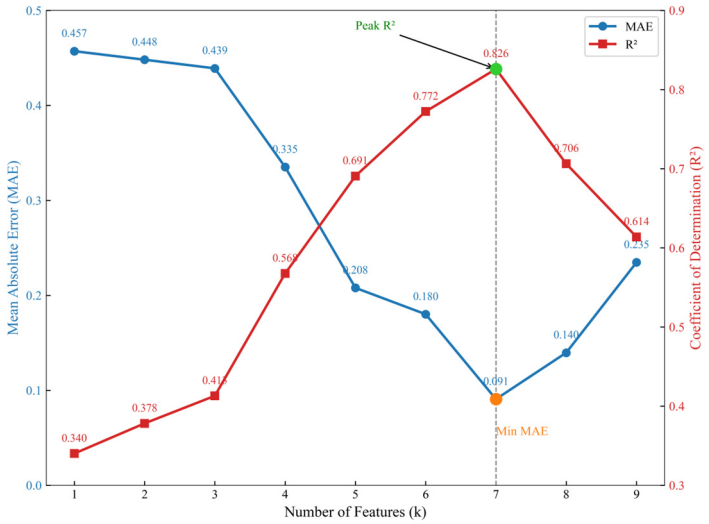

Figure 7. Relationship between number of features and model accuracy.

As shown in Figure 7, the number of features and the prediction performance of the hybrid model exhibit an inflection point: As the number of selected feature groups increases from 1 to 7, the model's

prediction accuracy improves significantly (MAE decreases, R^2 increases), reaching optimal performance with 7 features. The experimental results indicate that with fewer features, the input information is limited, making it difficult for the model to extract effective patterns, resulting in lower accuracy for predicting the shape parameter. As the number of features increases, more useful information is utilized, enhancing prediction performance; however, when the number of features exceeds 7, redundant information increases, interfering with the model's ability to learn key features and reducing prediction accuracy. These findings suggest that under multi-feature conditions, selecting a reasonable combination of key features with high MI is crucial for improving the performance of the MLP-RF hybrid model in predicting shape parameters. The seven final key features selected in this study are C4, C8, C10, C2, C15, C5, and C11.

According to the data processing sequence indicated by the red box in the flowchart of Figure 1, the processing results shown in Figures 4–7 and Table 2 are obtained. Based on these results, the feature selection process summarized in Table 3 is derived.

Table 3. Feature selection process and results.

Method	Feature ranking results	Number of features
VIF	C2,C13,C15,C4,C3,C8,C7,C10,C6, C5,C11,C1,C14,C9,C16,C12,C17	17
XGBoost	C4,C2,C5,C8,C11,C15,C10,C14,C7, C9,C3,C13,C6,C12,C16,C17,C1	17
Integration of VIF and XGBoost results	C2,C4,C5,C8,C9,C10,C11,C14,C15	9
Feature ranking results based on MI	C4,C8,C10,C2,C15,C5,C11,C9,C14	9
Prediction accuracy screening results of the MLP-RF model	C4,C8,C10,C2,C15,C5,C11	7

5. SSA-MLP-RF model construction

During hyperparameter optimization, the SSA introduces random perturbations in the search space for local exploration while guiding individual updates using the global optimal solution, achieving a balance between local search and global convergence. Through SSA parameter sensitivity analysis (as shown in Figure 8), considering both computational accuracy and runtime, the following settings are adopted: The algorithm is configured with a total of 60 sparrows and 50 iterations; in each iteration, the fitness of individuals is evaluated using the mean squared error on the validation set, and the top 20% of individuals are selected as discoverers. The iteration process terminates upon reaching the maximum number of iterations.

Through this optimization process, the final hyperparameter combination is obtained: The MLP model includes three hidden layers with 119 neurons per layer and a learning rate of 0.0428; and the RF model contains 232 decision trees, a maximum depth of 33, and a maximum of 3 features per node. This optimization strategy effectively enhances the prediction performance of the MLP-RF ensemble on the validation set.

To evaluate the optimization effect, an ablation study is conducted. The unoptimized base models

are combined into an MLP-RF model, while the optimized best-performing MLP and RF models are combined to form the SSA-MLP, SSA-RF, and SSA-MLP-RF models. The effectiveness of each improvement step is assessed by comparing the results of six performance metrics on the test set. The threshold setting determines the stability of the ensemble model. The validation set errors of the optimized single machine learning models are $MAE_v^{MLP} = 0.0872$ and $MAE_v^{RF} = 0.0791$, with $Q = 0.093$, which corresponds to the critical value of threshold θ.

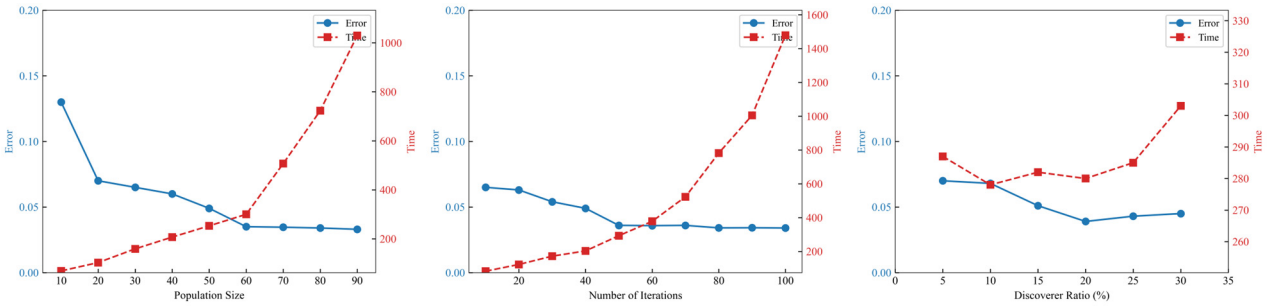

Figure 8. The SSA parameter sensitivity analysis results.

As shown in Table 4, the SSA-MLP-RF optimized ensemble model achieves the highest R^2 on the test set, followed by the MLP-RF ensemble model. Based on the error metrics, the SSA-MLP-RF optimized ensemble model exhibits the smallest errors, the highest prediction accuracy for the shape parameter, and the lowest Rényi entropy, indicating the most stable model outputs. Figure 9 presents the prediction performance of the trained model on a portion of the test set. The predicted values of the SSA-MLP-RF optimized ensemble model align closely with the ideal line, and the errors are randomly distributed around zero, demonstrating strong generalization capability and minimal systematic bias. The residuals are concentrated and approximately symmetric, indicating low random fluctuations and variance. In contrast, the residual distributions of the other models are wider and skewed, reflecting poorer fitting stability. Overall, the SSA-MLP-RF optimized ensemble model achieves higher accuracy and robustness in predicting the shape parameter.

Table 4. Comparative analysis of machine learning model metrics.

Model	R^2	MAE	RMSE	MAPE/%	NMSE	Rényi entropy
MLP	0.7986	0.0709	0.0919	10.5216	0.2014	0.2076
RF	0.8652	0.0652	0.0768	7.9428	0.1348	0.1732
MLP-RF	0.8895	0.0589	0.0622	5.9436	0.1105	0.1410
SSA-MLP	0.8172	0.0691	0.0871	8.7960	0.1828	0.1903
SSA-RF	0.8703	0.0607	0.0679	7.0315	0.1297	0.1679
SSA-MLP-RF	**0.9203**	**0.0391**	**0.0499**	**3.8201**	**0.0797**	**0.1200**

In this section, we present the construction and parameter optimization process of the SSA-MLP-RF model; however, its advantages over other metaheuristic algorithms require further validation. To address this, in the following section, we conduct a systematic comparative analysis to evaluate the superiority of the SSA-based optimization strategy in terms of predictive performance and stability.

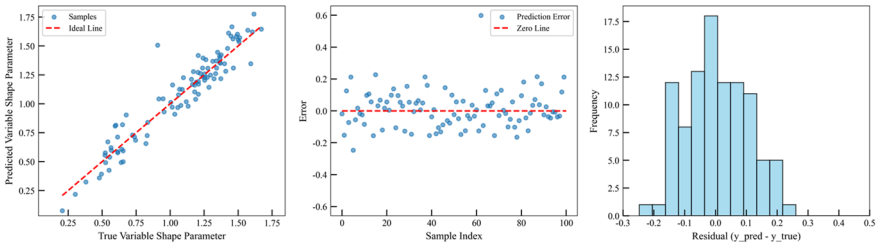

a. MLP model predictions, error plot, and residual histograms.

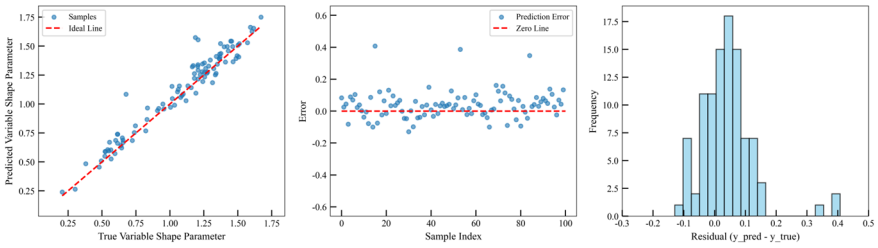

b. RF model predictions, error plot, and residual histograms.

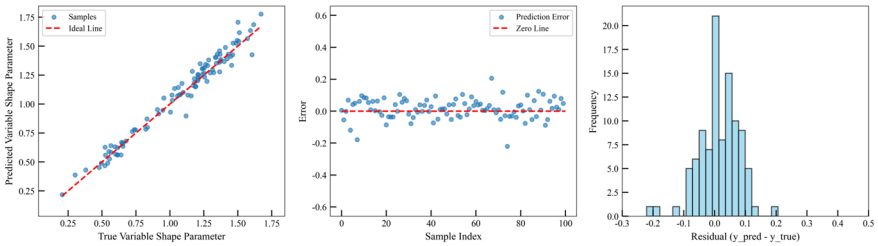

c. MLP-RF model predictions, error plot, and residual histograms.

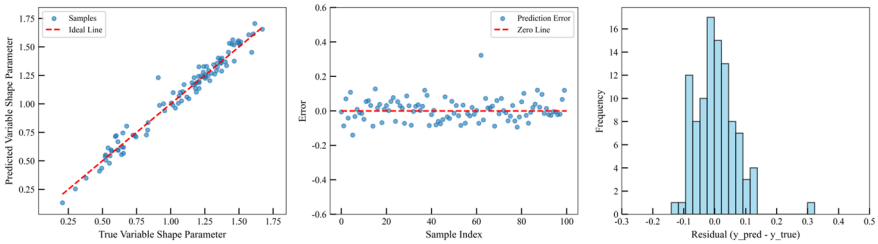

d. SSA-MLP model predictions, error plot, and residual histograms.

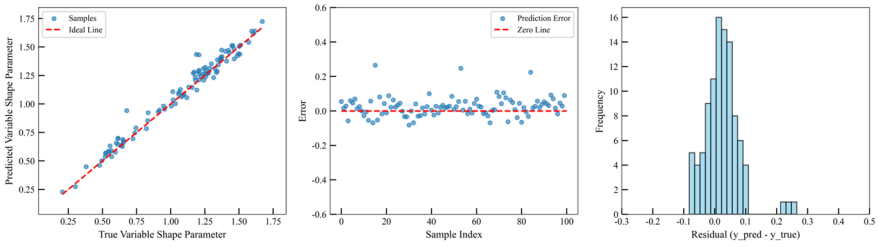

e. SSA-RF model predictions, error plot, and residual histograms

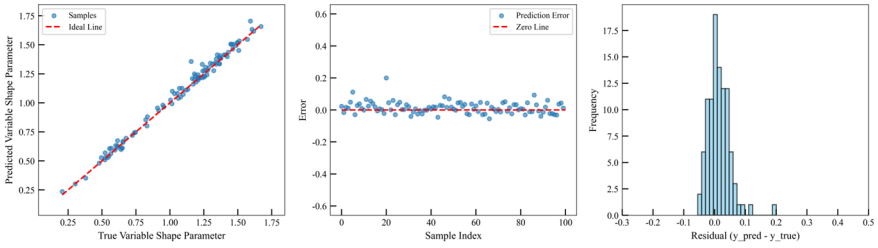

f. SSA-MLP-RF model predictions, error plot, and residual histograms.

Figure 9. Comparison of prediction performance among the six models.

6. Comparative analysis of different models

To further validate the effectiveness of the proposed SSA-MLP-RF hybrid optimization framework, SSA is compared with several classical metaheuristic algorithms, including PSO, GA, WOA, and BSLO. Each algorithm is combined with the same MLP-RF model for hyperparameter optimization and shape parameter prediction. By comparing prediction accuracy, goodness of fit, and stability under different optimization strategies, the advantages of the SSA-optimized model can be quantitatively and visually demonstrated. The comparative results of the algorithms are presented in Table 5, with the overall visualization shown in Figure 10, and the predictive performance of individual models illustrated in Figure 11.

Table 5. Comparison of performance indicators among models.

Model	R^2	MAE	RMSE	MAPE/%	NMSE	Rényi entropy
SSA-MLP-RF	**0.9203**	**0.0391**	**0.0499**	**3.8201**	**0.0797**	**0.1200**
BSLO-MLP-RF	0.9003	0.0403	0.0514	3.9347	0.0997	0.1236
PSO-MLP-RF	0.8993	0.0473	0.0529	4.0493	0.1007	0.1236
GA-MLP-RF	0.8907	0.0507	0.0601	4.2785	0.1093	0.1344
WOA-MLP-RF	0.8971	0.0498	0.0559	4.1639	0.1029	0.1308

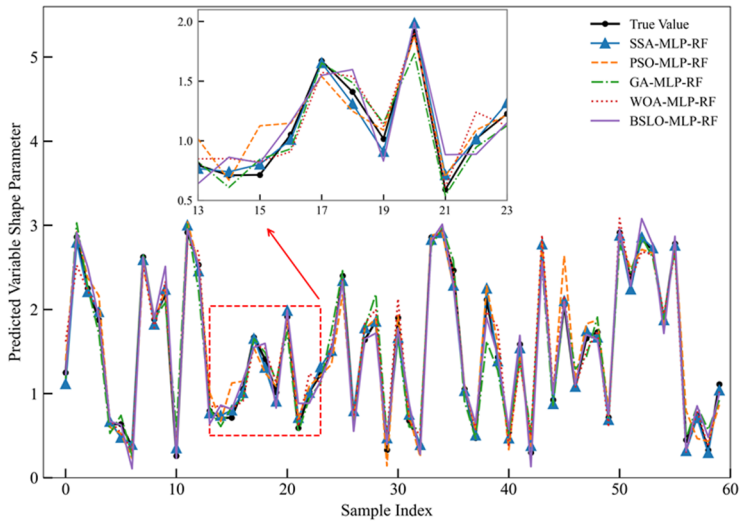

Figure 10. Overall predictive performance of the five models.

As shown in Table 5, the SSA-MLP-RF model achieves the best results across MAE, RMSE, MAPE, NMSE, and Rényi entropy, demonstrating superior prediction accuracy, stability, and generalization ability. In contrast, the GA-MLP-RF and WOA-MLP-RF models exhibit larger errors and higher uncertainty. Figures 10 and 11 visually confirm this conclusion, indicating that the SSA-based optimization strategy provides a more efficient parameter search capability within the hybrid framework.

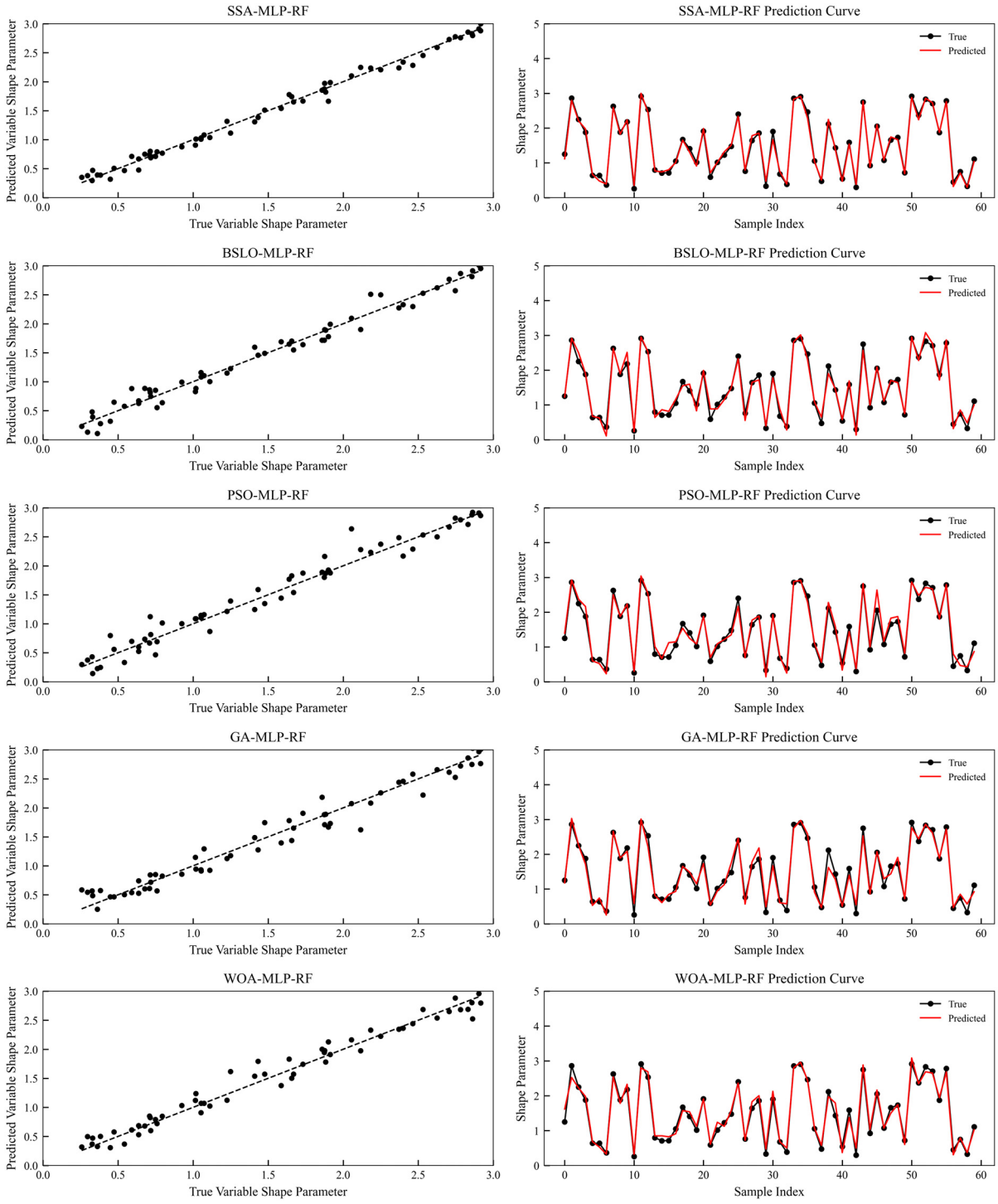

Figure 11. Comparison of prediction performance among models.

7. Conclusions

In this study, we proposed a geometry-driven framework for predicting variable shape parameters in IMQ-RBF interpolation. A large dataset linking local geometric features with optimal shape parameters was constructed using the SSA. Outlier removal, VIF analysis, XGBoost feature

importance, and MI analysis were employed to identify seven key local features, including the mean nearest-neighbor distance, neighborhood density, local curvature, absolute value of neighborhood linear fitting gradient, mean quadratic polynomial fitting error, dominant period corresponding to maximum amplitude of neighborhood discrete Fourier transform, and maximum triangle area. Based on these features, an SSA-optimized MLP-RF model was developed (MLP with three hidden layers of 119 neurons each and a learning rate of 0.0428; RF with 232 trees, maximum depth of 33, and a maximum of 3 features per node). The model achieved excellent performance on the test set (R^2 = 0.9203 MAE = 0.0391, RMSE = 0.0499, MAPE = 3.8201%, NMSE = 0.0797, Rényi entropy = 0.1200). Ablation experiments confirmed the effectiveness of the two-layer optimization strategy, while comparisons with PS, GA, WOA, and BSLO-based models further demonstrated the superior accuracy and stability of the SSA-MLP-RF approach.

In future work, we will focus on expanding the diversity of data types and integrating advanced geometric feature extraction and deep learning architectures to enhance model robustness and interpretability. Overall, the proposed framework provides an effective and extensible solution for adaptive shape parameter selection in RBF interpolation and establishes a foundation for integrating metaheuristic optimization with feature-driven learning in subsequent studies.

Use of AI tools declaration

The authors declare they have not used Artificial Intelligence (AI) tools in the creation of this article.

Acknowledgments

This research was supported by the National Natural Foundation of China (11601151).

Conflict of interest

The authors declare there is no conflict of interest.

References

1. Z. Wu, Radial basis function scattered data interpolation and the meshless method of numerical solution of PDEs, *J. Eng. Math.*, **19** (2002), 1–12.
2. J. Sun, L. Wang, D. Gong, Model for choosing the shape parameter in the multiquadratic radial basis function interpolation of an arbitrary sine wave and its application, *Mathematics*, **11** (2023), 1856. https://doi.org/10.3390/math11081856
3. S. Rippa, An algorithm for selecting a good value for the parameter c in radial basis function interpolation, *Adv. Comput. Math.*, **11** (1999), 193–210. https://doi.org/10.1023/a:1018975909870
4. J. Sun, L. Wang, D. Gong, An adaptive selection method for shape parameters in MQ-RBF interpolation for two-dimensional scattered data and its application to integral equation solving, *Fractal Fract.*, **7** (2023), 448. https://doi.org/10.3390/fractalfract7060448

5. J. Sun, W. Wang, A localized MQRBF-FD method with adaptive shape parameter optimization for acoustic wave simulation, *Eng. Anal. Bound. Elem.*, **177** (2025), 106270. https://doi.org/10.1016/j.enganabound.2025.106270
6. H. Nojavan, S. Abbasbandy, T. Allahviranloo, Variable shape parameter strategy in local radial basis functions collocation method for solving the 2D nonlinear coupled burgers' equations, *Mathematics*, **5** (2017), 38. https://doi.org/10.3390/math5030038
7. B. Fornberg, J. Zuev, The Runge phenomenon and spatially variable shape parameters in RBF interpolation, *Comput. Math. Appl.*, **54** (2007), 379–398. https://doi.org/10.1016/j.camwa.2007.01.028
8. J. A. Koupaei, M. Firouznia, S. M. M. Hosseini, Finding a good shape parameter of RBF to solve PDEs based on the particle swarm optimization algorithm, *Alex. Eng. J.*, **57** (2018), 3641–3652. https://doi.org/10.1016/j.aej.2017.11.024
9. D. Moazami, M. Esmaeilbeigi, Enhanced stability and accuracy in solving nonlinear Fredholm integral equations using hybrid radial kernels and particle swarm optimization, *Comput. Appl. Math.*, **44** (2025), 78. https://doi.org/10.1007/s40314-024-03039-0
10. F. Afiatdoust, M. Esmaeilbeigi, Optimal variable shape parameters using genetic algorithm for radial basis function approximation, *Ain Shams Eng. J.*, **6** (2015), 639–647. https://doi.org/10.1016/j.asej.2014.10.019
11. F. N. Mojarrad, M. H. Veiga, J. S. Hesthaven, P. Öffner, A new variable shape parameter strategy for RBF approximation using neural networks, *Comput. Math. Appl.*, **143** (2023), 151–168. https://doi.org/10.1016/j.camwa.2023.05.005
12. J. Sun, W. Wang, Optimizing shape parameters in RBF methods: A systematic review of techniques, applications, and computational challenges, *Comput. Sci. Rev.*, **59** (2026), 100842. https://doi.org/10.1016/j.cosrev.2025.100842
13. P. González-Rodelas, H. M. H. Idais, M. Yasin, M. Pasadas, Optimal centers' allocation in smoothing or interpolating with radial basis functions, *Mathematics*, **10** (2021), 59. https://doi.org/10.3390/math10010059
14. A. H. Bacar, S. C. Rawhoudine, An optimal multiquadric variable shape parameter for boundary value problems using particle swarm optimization, *J. Math. Res.*, **16** (2024), 108–131. https://doi.org/10.5539/jmr.v16n2p108
15. M. Heidari, M. Mohammadi, S. De Marchi, Curvature based characterization of radial basis functions: Application to interpolation, *Math. Model. Anal.*, **28** (2023), 415–433. https://doi.org/10.3846/mma.2023.16897
16. S. Xiang, K. Wang, Y. Ai, Y. Sha, H. Shi, Trigonometric variable shape parameter and exponent strategy for generalized multiquadric radial basis function approximation, *Appl. Math. Modell.*, **36** (2012), 1931–1938. https://doi.org/10.1016/j.apm.2011.07.076
17. J. Biazar, M. Hosami, Selection of an interval for variable shape parameter in approximation by radial basis functions, *Adv. Numer. Anal.*, **2016** (2016), 1397849. https://doi.org/10.1155/2016/1397849
18. S. Zhu, A. J. Wathen, Convexity and solvability for compactly supported radial basis functions with different shapes, *J. Sci. Comput.*, **63** (2015), 862–884. https://doi.org/10.1007/s10915-014-9919-9
19. M. Bozzini, L. Lenarduzzi, M. Rossini, R. Schaback, Interpolation with variably scaled kernels, *IMA J. Numer. Anal.*, **35** (2015), 199–219. https://doi.org/10.1093/imanum/drt071

20. M. A. Jankowska, A. Karageorghis, Variable shape parameter Kansa RBF method for the solution of nonlinear boundary value problems, *Eng. Anal. Boundary Elem.*, **103** (2019), 32–40. https://doi.org/10.1016/j.enganabound.2019.02.005
21. S. N. Chiu, L. Ling, M. McCourt, On variable and random shape Gaussian interpolations, *Appl. Math. Comput.*, **377** (2020), 125159. https://doi.org/10.1016/j.amc.2020.125159
22. Y. Zhang, J. Lin, S. Reutskiy, A novel Gaussian-cubic-based backward substitution method using symmetric variable shape parameter, *Eng. Anal. Boundary Elem.*, **155** (2023), 1069–1081. https://doi.org/10.1016/j.enganabound.2023.07.026
23. S. Lin, D. L. Young, C. Chen, Ghost-point based radial basis function collocation methods with variable shape parameters, *Eng. Anal. Boundary Elem.*, **130** (2021), 40–48. https://doi.org/10.1016/j.enganabound.2021.05.006
24. J. Yu, Z. Lei, Q. Yao, F. Zhou, X. Pan, A bounded randomly variable shape multi-quadric interpolation method in dual reciprocity boundary element method, *Eng. Anal. Boundary Elem.*, **134** (2022), 377–387. https://doi.org/10.1016/j.enganabound.2021.10.001
25. Z. Majdisova, V. Skala, M. Smolik, Algorithm for placement of reference points and choice of an appropriate variable shape parameter for the RBF approximation, *Integr. Comput. Aided Eng.*, **27** (2020), 1–15. https://doi.org/10.3233/ica-190610
26. K. Gao, G. Mei, S. Cuomo, F. Piccialli, N. Xu, ARBF: adaptive radial basis function interpolation algorithm for irregularly scattered point sets, *Soft Comput.*, **24** (2020), 17693–17704. https://doi.org/10.1007/s00500-020-05211-0
27. J. Bai, H. Nguyen-Xuan, E. Atroshchenko, G. Kosec, L. Wang, M. A. Wahab, Blood-sucking leech optimizer, *Adv. Eng. Software*, **195** (2024), 103696. https://doi.org/10.1016/j.advengsoft.2024.103696
28. F. Wei, Y. Feng, X. Shi, K. Hou, Improved sparrow search algorithm with adaptive multi-strategy hierarchical mechanism for global optimization and engineering problems, *Cluster Comput.*, **28** (2025), 215. https://doi.org/10.1007/s10586-024-04883-9
29. X. Guo, F. Ding, Y. Han, Diffusion residual graph neural network-based model for XSS detection, *Comput. Eng. Des.*, **46** (2025), 2888–2894. https://doi.org/10.16208/j.issn1000-7024.2025.10.020

AIMS Press